A High-Speed Adaptive Antenna Array With Simultaneous Multibeam-Forming Capability

Takahide Nishio, *Student Member, IEEE*, Hsiao-Ping Tsai, *Member, IEEE*, Yuanxun Wang, *Member, IEEE*, and Tatsuo Itoh, *Fellow, IEEE*

***Abstract*—A new type of adaptive beamforming antenna system architecture is proposed for multichannel wireless communications. Multibeam communication with high data throughput is accomplished using the proposed beamformer architecture. The system consists of analog mixers, a multitone direct digital synthesizer (DDS), and a digital signal processor (DSP) controller. The essential idea of multibeam forming is based on a multitone weighting scheme combined with analog–digital hybrid signal processing. While the real-time multibeam construction is realized by the analog mixer circuits and a DDS, the complicated adaptive beamforming and direction-of-arrival estimation algorithms are carried out by the DSP. In this architecture, only one beamformer circuit is required to handle multiple beams, leading to significant reduction in hardware counts. A 5.8-GHz eight-element adaptive beamforming array successfully demonstrates two-beam simultaneous beamforming with less than three degrees of peak and null steering errors and more than 20-dB interference suppression. The test-bed exhibits successful two-channel data recovery at 25-Mb/s data throughput in each channel with binary phase-shift keying modulation, for simultaneous dual-beam reception. The bit-error-rate measurement validates the robustness of the communication quality under strong interferences.**

***Index Terms*—Adaptive arrays, microwave communication, multibeam antennas, space division multiplexing.**

I. Introduction

ADAPTIVE beamforming arrays provide flexible antenna pattern control and simultaneous multibeam transmitting and receiving capabilities [1], [2]. Multibeam adaptive arrays can enhance the performance of wireless systems in terms of capacity, coverage, and throughput by spatial filtering [2]–[4]. Conventional adaptive array systems utilize a fully digital signal-processing approach to accomplish the data modulation, coding, and beamforming [5]–[7]. However, when multiple beams are required, these systems suffer from I/O and computation speed limits of the digital circuits. In current technology, high-speed analog-to-digital (A/D) converters with more than gigabit-per-second sampling are available and they satisfy the throughput speed in most multichannel or multibeam communications. The issues rather come from the overall throughput speed of the digital signal processor (DSP), which is usually much slower than its sampling clock speed, due to the use of oversampling and the response speed limit of digital gates. In addition, the DSP has a first-in–first-out (FIFO) buffer memory system to store a certain amount of data in a fixed period before processing. This introduces a significant amount of processing delay that prevents the DSP from operating in real time. Moreover, separate beamforming networks and data modulation blocks are required to form a number of beams simultaneously, multiplying the computation load. These multichannel throughput tasks at the DSP, connected in series to the RF front-end, lower the processing speed proportional to the number of channels and elements.

On the other hand, in analog beamforming systems combined with DSP for parallel weighting computation, high data throughput can be realized even in multichannel signal processing since the real-time beamforming tasks are carried out not by DSP, but by analog multipliers combined with heterodyne quadrature down-converters [8]. In this way, the application of weighting vectors is performed as a throughput in real time by analog circuits. These are free from the clock and memory delays that would be incurred if the same functions were to be realized entirely with DSP. The computation task of updating weighting vectors can be performed slow enough to fall within the current speed limit of the DSP throughput in order to track moving targets in real time. A/D converters are only used to sample the data intermittently for direction-of-arrival (DOA) estimation, which does not require high DSP throughput. The A/D sampling rate requirement is the same in either multibeam or single-beam operation. For extremely high data rates, the sub-band sampling technique [9] can be used to overcome A/D speed limits. In spite of all these advantages, this analog–digital hybrid beamforming architecture requires a separate set of beamforming circuits for each synthesized beam [8]. Thus, it becomes unaffordable for multichannel (or multibeam) beamforming applications such as base-station antennas where more than ten beam outputs are required.

To develop a high-speed adaptive-beamforming smart antenna system with simultaneous multibeam-forming capability, we propose a novel array architecture using a combination of analog and digital processing circuits with the addition of a direct digital synthesizer (DDS) to generate multitone weightings. The approach offers advantages in both operating speed and complexity compared to conventional digital and analog/digital beamforming techniques in multibeam scenarios. The system uses an analog beamformer to realize real-time high-speed throughput that maintains nonstop signal flow for multichannel data communications. Thus, the DSP only operates for the computation intensive tasks such as DOA

Manuscript received April 16, 2003. This work was supported by the University of California under the Discovery Program.

T. Nishio, Y. Wang, and T. Itoh are with the Department of Electrical Engineering, University of California at Los Angeles, Los Angeles, CA 90095-1594 USA (e-mail: itoh@ee.ucla.edu).

H.-P. Tsai is with Mindspeed Technologies, Newport Beach, CA 92660 USA.

Digital Object Identifier 10.1109/TMTT.2003.819770

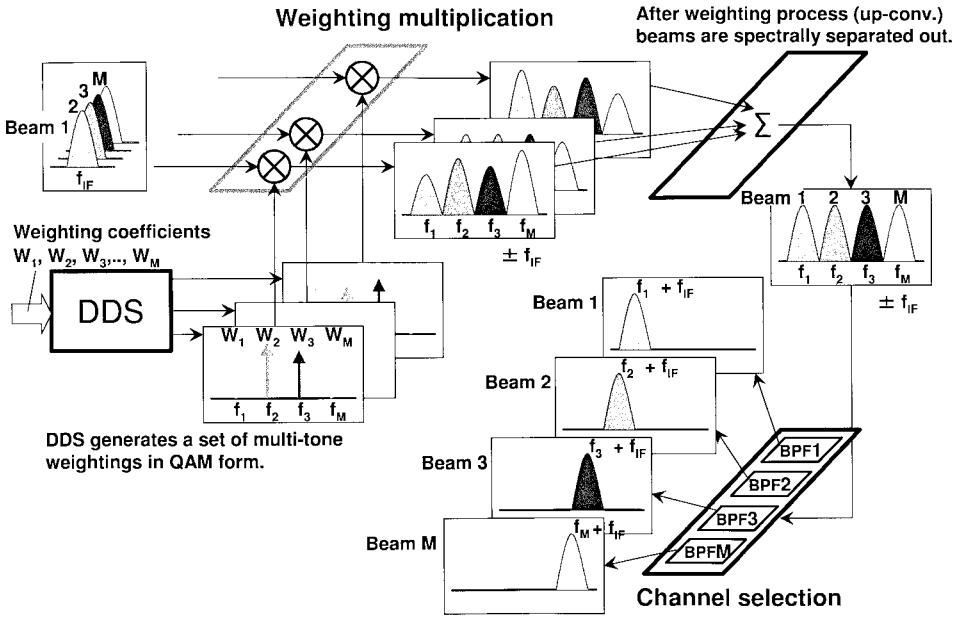

Fig. 1. Multitone weighting scheme used for the proposed multibeam beamformer.

estimation and weighting computation. In addition, the use of our multitone weighting scheme reduces the number of operation units from $M \times N$ to $M + N$ in the case of an M-beam scenario using an N-element system. The crucial part of the system is a real-time beamformer consisting of analog mixers and a DDS. Fig. 1 shows the signal flow of the multibeam beamformer based on a new concept called the multitone weighting scheme. The DDS generates a set of multitone signals where the amplitude and phase of each tone correspond to one of the complex weighting coefficients. These coefficients are then applied in the weighting process, which is accomplished through modulation using analog mixers. The application of multiple weighting coefficients can be executed in a single mixer since the local-oscillator (LO) signal supplied from the DDS consists of multiple tones. This is similar to the idea of the frequency-division multiple-access (FDMA) scheme used in wireless communication. For this reason, multiple antenna beams can be formed without much increase in hardware expenses. After beamforming, those channels can be flexibly selected using bandpass filters (BPFs). The selected channel signals are recovered by demodulation using the corresponding multitone carriers.

This paper is organized as follows. First, the system concepts and simulated results for the proposed multibeam beamformer are introduced. The measured component performances of the RF front-end and multibeam beamformer are then given as a circuit overview. Finally, the measured system performance including DOA estimation error, two-channel adaptive beamforming, data recovery, and bit-error rate (BER) performance is presented to validate the original concept.

II. Multibeam Beamformer Concept

Fig. 2 shows the block diagram of the proposed multibeam adaptive array. It is assumed that the M-channel RF signals sharing a common RF carrier with different baseband data are incoming from different directions. First, the received M-channel RF signals in the N element antenna array are down-converted to low-IF signals. The IF signal at the nth element is expressed as

$$s_{\mathrm{IF}\,n}(t) = \sum_{m=1}^{M} \left(b_m(t) \cos(\omega_{\mathrm{IF}} t + \phi_{m,n}) \right) \tag{1}$$

where ω_{IF} is the angular frequency of the IF signal, $b_m(t)$ is the baseband data of the mth channel, and $\phi_{m,n}(t)$ is the phase of the mth channel IF signal at nth element. The IF signals are then split into two paths; one goes to the DSP controller and the other to analog mixers in the beamformer. In the DSP controller, the IF signals are sampled at the A/D converter. $(M \times N)$ sets of weighting coefficients are subsequently computed at the DSP based on the sampled IF signals. In a traditional multibeam construction architecture, $(M \times N)$ sets of multiplication components would be needed for vector weighting process. However, in the proposed architecture, the same weighting function is accomplished at an expense of only $(M+N)$ sets of analog mixers due to our use of the FDMA concept.

The M-tone I/Q DDS plays an important role in this multiplication process. The main role of the DDS is to modulate the M-channel weighting coefficient sets onto M-tone carriers in quadrature-amplitude-modulation (QAM) form. The time-domain DDS output signal at the nth element is expressed as

$$s_{W\,n}(t) = \sum_{m=1}^{M} \left(Wr_{m,n} \cos \omega_m t + Wi_{m,n} \sin \omega_m t \right) \tag{2}$$

where Wr and Wi represent real and imaginary components of complex weighting coefficients and ω_m is the carrier frequency for the mth channel. In the proposed beamformer, the vector multiplication of the M-tone weightings from the DDS and N-element IF signals from the down-converter is carried

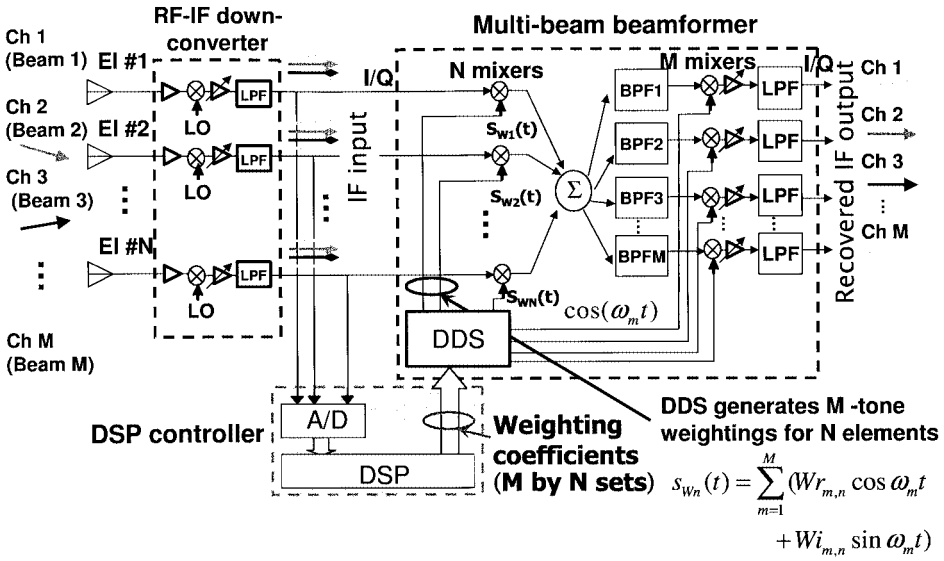

Fig. 2. Proposed multibeam adaptive-beamforming receiver system block diagram.

out by N analog mixers. Assuming each mixer works as an ideal multiplier, the output signal of the nth element mixer is expressed as

$$\begin{aligned} s_n(t) &= s_{W\,n}(t) \times s_{\mathrm{IF}\,n}(t) \\ &= \sum_{m=1}^{M} \left(Wr_{m,n} \cos \omega_m t + Wi_{m,n} \sin \omega_m t\right) \\ &\qquad \times \sum_{m=1}^{M} \left(b_m(t) \cos(\omega_{\mathrm{IF}} t + \phi_{m,n})\right). \end{aligned} \tag{3}$$

Once this multiplication is done at each mixer, the IF signals are not only weighted to form M independent beams, but also up-converted to M-channel frequencies. The weighting vector summation is subsequently carried out using an N-way power combiner where the multitone weighting process is completed as follows:

$$\begin{aligned} s_{\mathrm{out}}(t) &= \sum_{n=1}^{N} \left(s_{W\,n}(t) \times s_{IF\,n}(t)\right) \\ &= \sum_{n=1}^{N} \left(\sum_{m=1}^{M} \left(Wr_{m,n} \cos \omega_m t + Wi_{m,n} \sin \omega_m t\right) \right. \\ &\qquad \left. \times \sum_{m=1}^{M} \left(b_m(t) \cos(\omega_{\mathrm{IF}} t + \phi_{m,n})\right) \right). \end{aligned} \tag{4}$$

The factored form of (4) contains both sidebands along $\omega_m \pm \omega_{\mathrm{IF}} (m = 1, 2, \ldots, M)$. Both upper sideband (USB) and lower sideband (LSB) components contain only mth channel baseband information $b_m(t)$ from the multitone weighting multiplication process, but their phase polarities upon weighting are inverse with respect to each other. Thus, one of the sidebands must be eliminated with subsequent BPFs to prevent image beam detection.

After this weighting process, M sets of BPFs are used for channel selection. In the prototype, only the USB component at frequency $\omega_m + \omega_{\mathrm{IF}} (m = 1, 2, \ldots, M)$ is selected in each channel to hold the positive phase polarity upon weighting. The spectrally separated signals are then down-converted by the corresponding carrier frequencies $\omega_m (m = 1, 2, \ldots, M)$ using M analog mixers. The IF signals are finally recovered using low-pass filters (LPFs) where the unwanted harmonic components are removed. The baseband signals are obtained using any standard IF receiver in the subsequent stage.

Thus, the proposed multibeam beamformer can reduce the number of mixers from $(M \times N)$ to $(M + N)$ for weighting multiplication process. In addition, the down-conversion does not require the IF signals to be separated into in-phase (I) and quadrature-phase (Q) signals because the DDS can generate the complex form of the weightings in QAM. Since the I/Q down-converter and I/Q mixers for the weighting process are not required, the number of mixers is further reduced by a factor of two. This results in a simple and cost-effective down-converting and beamforming architecture for multibeam beamforming applications.

The M-channel multibeam beamformer can create M sets of independent beams pointing toward signals of interest (SOIs) by providing maximum gain to each estimated DOA. Meanwhile, the beamformer also suppresses interference and multipath signals by creating up to $(M - 1)$ sets of distinct nulls toward signals not of interest (SNOIs).

III. Simulated Results

The simulation of a four-channel multibeam beamformer with eight elements is carried out using a mathematical model in MATLAB. The simulation scenario is that the down-converted IF signals simultaneously received from four different directions (-20°, 0°, $+10^\circ$, and $+30^\circ$) are fed into the eight-element inputs of the multibeam beamformer. It is assumed that these IF signals include different baseband data (pseudonoise (PN) random codes for channels 1 and 2 and tone signals for channels 3 and 4), but shares a common IF carrier frequency at 33 MHz. At the DSP controller, the weighting coefficients for each channel are computed after the DOA estimation by

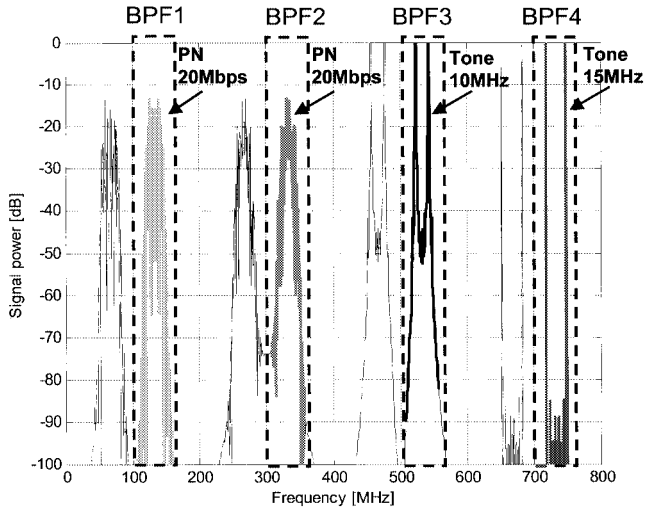

Fig. 3. Simulated output spectrum of the weighted sum before and after BPFs.

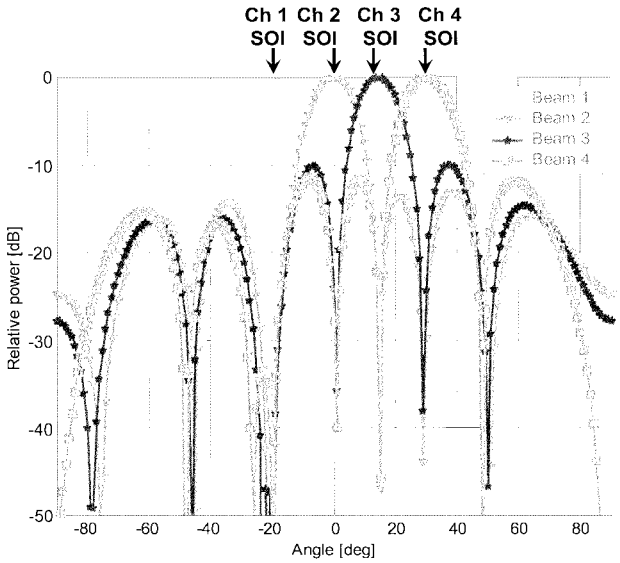

Fig. 4. Simulated beamforming results from the recovered IF signals.

the ESPRIT algorithm. The DDS subsequently generates the four-tone quadrature weightings that include amplitude and phase information for main-beam and null steering. The carrier frequencies for respective channels are 100, 300, 500, and 700 MHz.

After the weighting vectors are multiplied, the original IF signals from four different directions are up-converted onto those four tones and summed among different antenna elements. The weighted signal spectrum is shown in Fig. 3. From the spectrum, it is clearly observed that each up-converted signal contains corresponding baseband data only for a desired SOI channel since it is properly weighted. This indicates successful multibeam construction process. The individual BPF subsequently selects a USB component of the desired channel from the spectrally separated (four-tone) up-converted signals, as is also shown in Fig. 3. To prevent image beam detection and inter-channel crosstalk, it is necessary for the BPFs to provide fine filtering of undesired frequency components. Each BPF is also required to have a flat and wide passband to pass the IF bandwidth in order to prevent additional signal distortion in the mux/demux process. Finally, for the channel recovery, each signal is down-converted by multiplying the corresponding tone at the second-stage mixer, and filtering out the harmonic components with an LPF.

Fig. 4 shows the simulated four-channel adaptive beamforming results. The recovered IF signals are used to plot these beams. It is observed that each recovered IF signal forms a peak toward the intended SOI direction. At the same time, it exhibits nulls toward the angles of three other interference signals with respect to each other. The mathematical model in MATLAB validates the simultaneous multiple-beam forming capability of the proposed beamformer architecture. Fig. 5 shows the recovered baseband data in the respective channels plotted with original baseband data in the simulation. The baseband data are successfully demodulated back into four channels without loss of information. Since the ideal components are used to represent analog mixers, combiner/dividers, and filters, signal distortions due to time-delay response, nonlinear effects, unwanted harmonics, and intermodulations are not observed in the recovered baseband data.

IV. Circuit Overview

A multibeam adaptive array system consisting of a planar antenna array, RF–IF down-converter, and beamformer has been developed to validate the proposed concept experimentally. The test-bed with an eight-element linear array is capable of two-channel simultaneous beamforming and data recovery based on the space-division multiple-access (SDMA) concept ($M = 2$, $N = 8$).

A. RF Front-End and Phase Calibration

Fig. 6 shows the RF front-end consisting of a broad-band quasi-Yagi array [10] and an RF-IF down-converter.

The RF–IF down-converter consists of three-stage RF low-noise amplifiers (LNAs) with 34.5-dB gain, RF mixers with 9.5-dB conversion loss at $+10$-dBm LO power, IF variable gain amplifiers (IF VGAs) with up to 25-dB gain, and LPFs. For -50-dBm RF input power at 5.8 GHz, the IF signal power is boosted up to 0 dBm at 30 MHz by the IF VGAs. The IF VGAs are used to calibrate gain errors among elements of the IF signals.

The phase errors of the down-converter outputs are calibrated using sampled IF signals before weighting computation. This is done since they significantly affect the DOA estimation error and introduce degradations in the final beamforming patterns such as misalignment of peaks and nulls, as well as increased sidelobe levels. Considerable shifts in null locations may also result, which can severely impair the degree of interference suppression. In measurement, the circuit phase errors between adjacent elements are calibrated by receiving the RF signal from the broadside direction. In this case, it is expected that RF input signals arrive in-phase so that the IF output signals are also in-phase. Since circuit phase errors are expected to be constant, these fixed phase deviations are corrected to be in-phase by multiplying them with their own antiphase factors. The antiphase factors, i.e. phase-calibration factors, are obtained by detecting the phase of the sampled signals at the IF frequency using the Fourier transform.

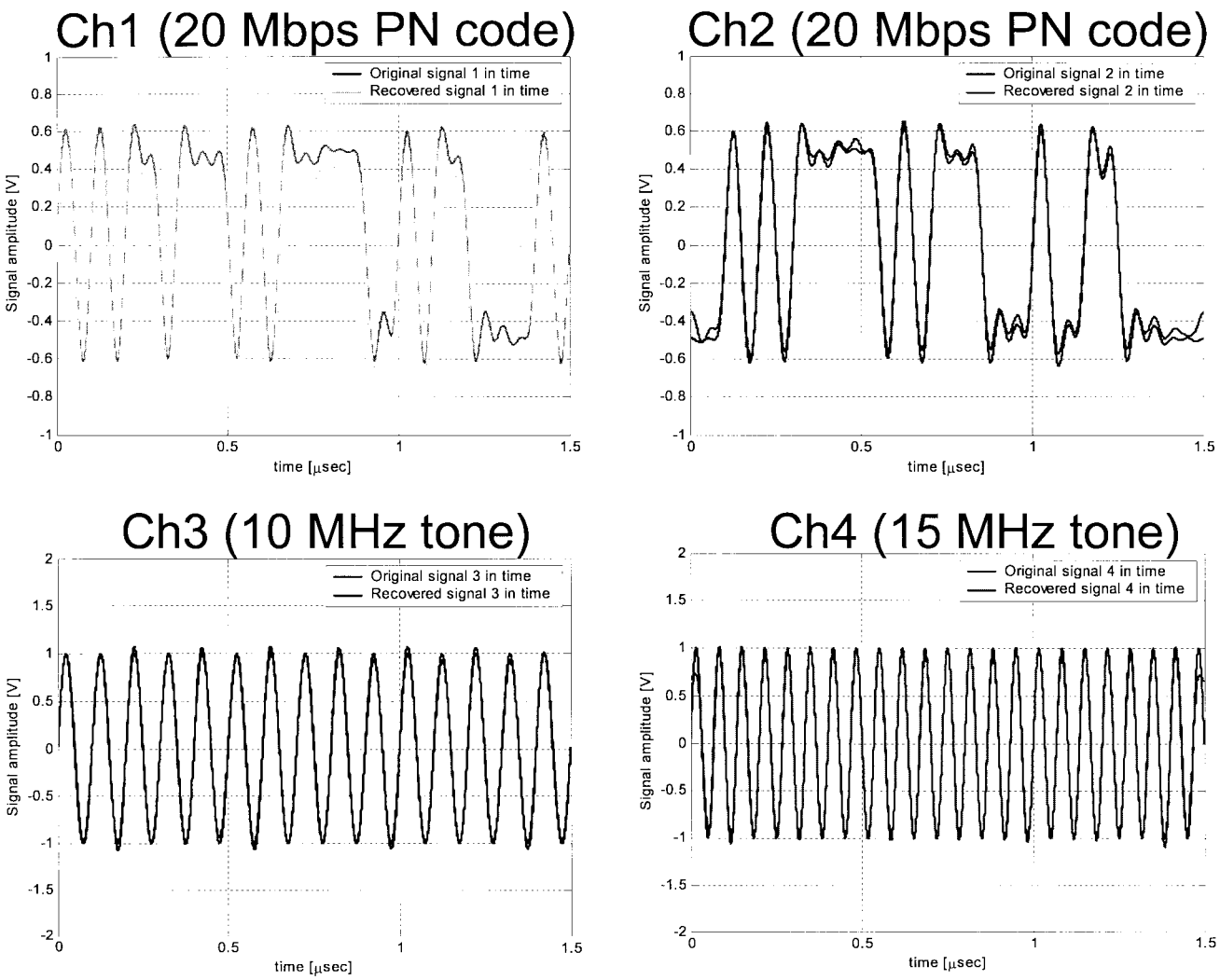

Fig. 5. Recovered baseband data plotted with the original data in simulation.

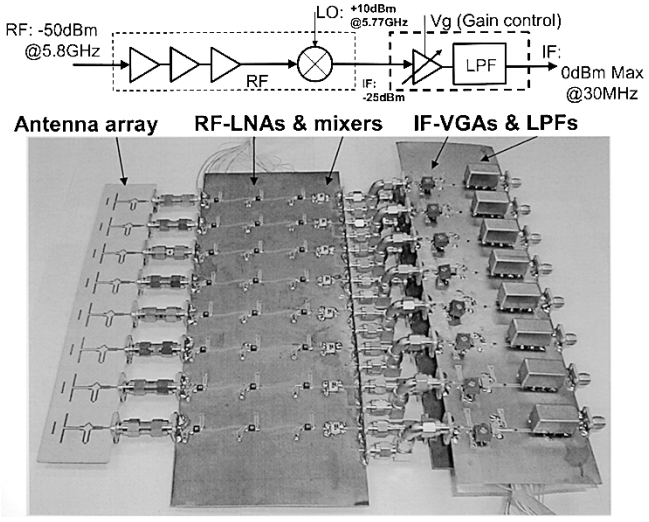

Fig. 6. RF front-end.

Fig. 7 shows the sampled IF signals before and after phase calibration. Before phase calibration, although the amplitude errors are corrected by the gain calibration at the IF VGAs, the phase deviation among elements is observed to be around 30° due to the circuit phase errors. However, after phase calibration, the circuit phase errors are significantly reduced within 1° so that enhancement of DOA estimation is expected.

Fig. 8 shows the estimated beamforming plots with and without phase calibration when the RF signal from the broadside direction is received. After the phase calibration, since the computed weighting coefficients are not influenced by the circuit phase errors of sampled IF signals, the uncalibrated main-beam peak, which is shifted 2° from the broadside direction due to the circuit phase errors, is corrected, and the distorted beam pattern shape becomes symmetric. This phase-error calibration of the RF front-end is carried out before each measurement in this paper. The phase-calibration factors are always applied in the calculation algorithm before DOA estimation and weighting computation to minimize final peak and null steering errors.

B. Multibeam Beamformer

Fig. 9 shows the multibeam beamformer including the analog beamformer and two-tone I/Q DDS. The two-tone I/Q DDS architecture is constructed using 8-bit D/A converters, differential

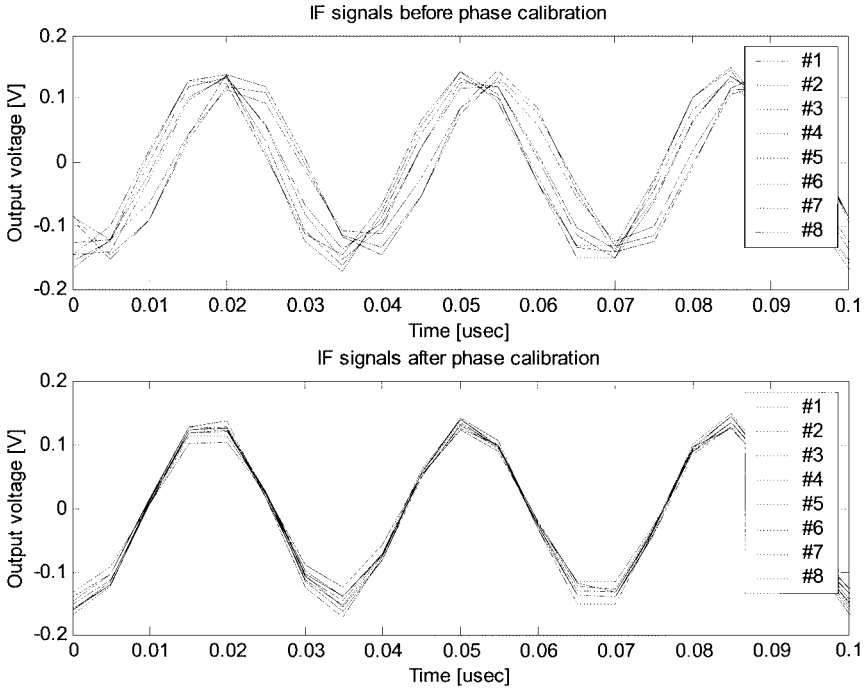

Fig. 7. Sampled IF signals before and after phase calibration.

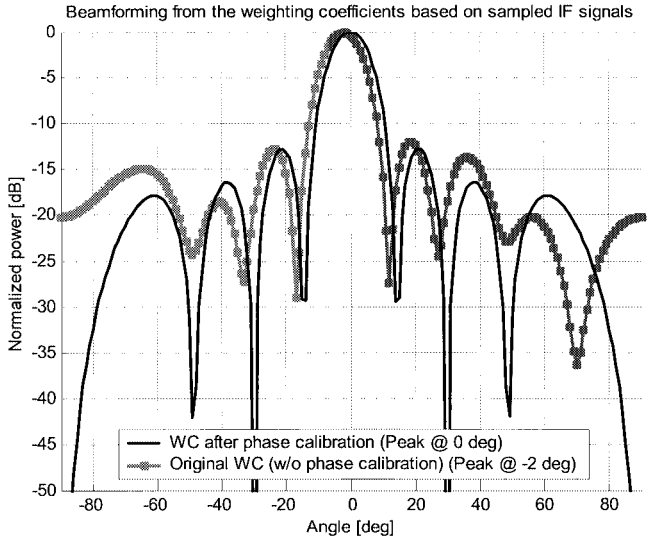

Fig. 8. Estimated beamforming patterns with and without phase calibration.

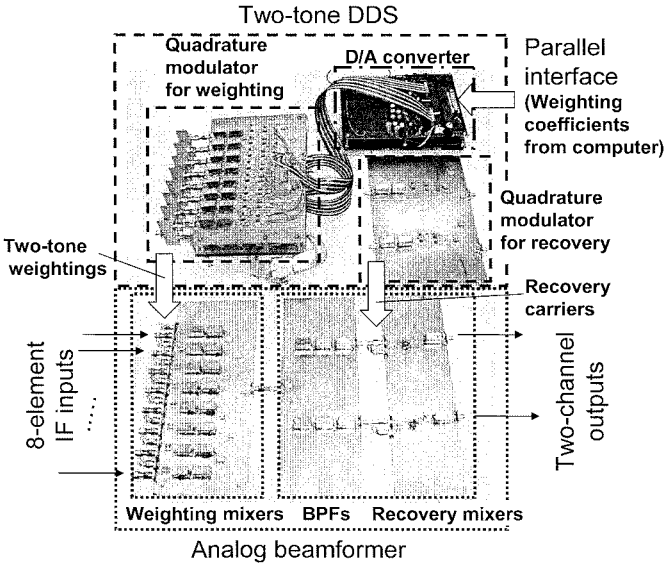

Fig. 9. Multibeam beamformer.

amplifiers, quadrature modulators, and BPFs. (2×8) sets of the computed weighting coefficients (for two channels, I/Q pair, and eight elements) in the DSP are directly applied in digital form to the DDS, where two-tone quadrature weightings for eight elements are generated. The two-tone carrier frequencies are 230 and 390 MHz, respectively. The recovery quadrature modulator is used to provide a synchronized LO source in channel recovery process.

Although the DDS architecture in this prototype is constructed using a number of components, the whole structure can be integrated into one chip in current DDS technology.

The analog beamformer mainly consists of weighting mixers (for up-conversion), channel-selection BPFs, and recovery mixers (for down-conversion). Passive analog mixers operating from dc to 650 MHz are used to provide good output linearity on weighting and recovery. The analog beamformer includes three-stage wide-band BPFs with 1-dB passband of 230–260 MHz for channel 1 and 390–420 MHz for channel 2. For fine channel selection and image beam cancellation, these BPFs provide over 40-dB inter-channel suppression and 20-dB LSB suppression. The output stage of the recovery mixer includes a single-stage IF VGA with up to 40-dB gain and an LPF with 3-dB cutoff at 33 MHz to retain high SNR channel outputs.

In the experiment, the A/D converter for sampling and the DSP for weighting computation are replaced by an eight-channel digital oscilloscope with 200-Ms/s sample

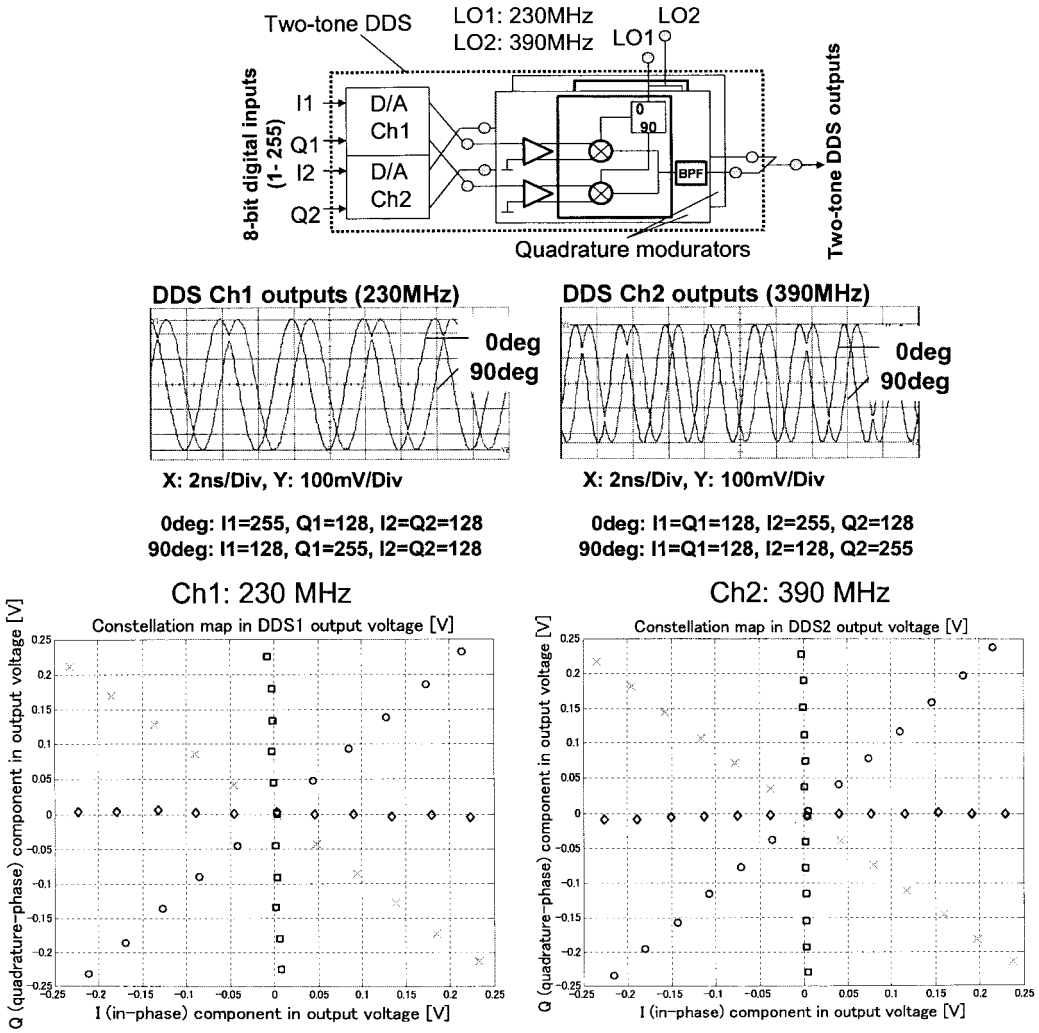

Fig. 10. Constellation plots of the two-tone DDS output at 230 (Ch1) and 390 MHz (Ch2).

rate and a personal computer, respectively. The sampled IF signals at the digital oscilloscope are digitally transferred to the computer through a general-purpose interface bus (GPIB) interface. The DSP function is carried out by MATLAB. The weighting computation in MATLAB is implemented in the following manner. The quadrature components of the sampled eight-element IF signals are first obtained using the Hilbert transform. The DOA estimation is then carried out using one of the standard algorithms, i.e., ESPRIT [11]. In ESPRIT, the signal subspace is divided into two sets of sensor subarrays that possess the displacement invariance. The phase information of the received signals is extracted by finding the phase of the complex roots from the eigenvalues, which are obtained using the rotational invariance relation of the subarrays. The DOA information is thus directly produced in terms of generalized eigenvalues. Finally, the sample matrix inversion (SMI) algorithm [12] is used to compute complex weighting coefficients for main-lobe steering toward SOIs and for nulling toward SNOIs. After being corrected with the phase-calibration factors, these weighting coefficient sets are digitally transferred from the computer to the D/A converter in the DDS through a parallel interface.

C. Two-Tone I/Q DDS Performance

Since the DDS generates the multitone weightings to perform peak and null steering for multiple beams, the performance of the DDS outputs directly affects the beamforming accuracy. To minimize I/Q amplitude errors, the calculated weighting coefficients at the computer are normalized and quantized to 8-bit digital values and then transferred to two 8-bit D/A converters. Each D/A converter drives eight quadrature modulators for each channel and generates maximum analog voltage swings of ± 0.3 V with an offset voltage of $+0.023$ V within 1-mV accuracy. These maximum swings and offset voltage are optimized such that quadrature modulators provide the best performance on I/Q amplitude linearity and zero output in 65 536 (256×256)—QAM at 230 and 390 MHz.

Fig. 10 shows the constellation plots of the two-tone DDS outputs at 230 MHz (Ch1) and 390 MHz (Ch2) when the input I or/and Q signals, digitally applied from the computer to the D/A converters, create the output phase of 0°, 45°, 90°, and 135° (each $\pm 180°$). The inputs are the quantized I/Q digital values ranging from 1 (providing a negative-phase maximum output) to 255 (providing a positive-phase maximum output), where 128

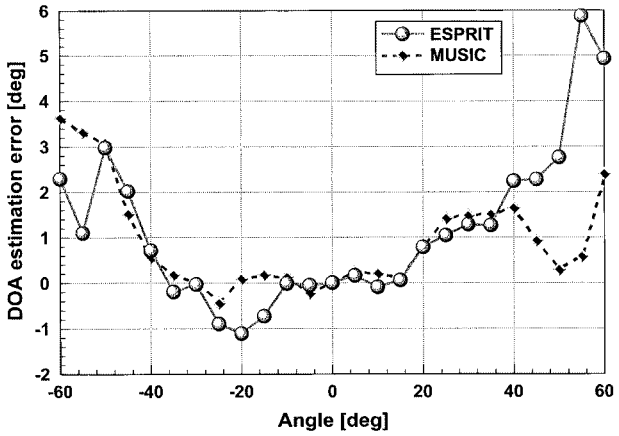

Fig. 11. Measured DOA estimation errors from ESPRIT and MUSIC in a single transmitter.

corresponds to the zero output. Only 13 amplitude points of I/Q combinations are plotted in Fig. 10. The input-to-output amplitude error is less than 0.5%. Excluding the zero output, the maximum phase error is less than 3°, where minimum and maximum digital values are simultaneously applied to the I and Q inputs to create output phases of 45° and 135° (±180°).

In addition, the gain error between channels (230 and 390 MHz) is less than 0.5 dB and the phase error among elements is less than 10°. These errors can be corrected by calibration factors. Thus, overall scan angle error caused by weighting process at the DDS is negligibly small.

V. Measured System Performance

A. DOA Estimation Error

The DOA estimation is carried out using two standard algorithms, i.e., ESPRIT and MUSIC [13] in the open space of a laboratory room. Fig. 11 shows DOA estimation error from $-60°$ to $+60°$ incident angle when a single-transmitter source is detected. In both algorithms, the DOA error is less than 3° within $\pm 50°$ incident angle, and rapidly degrades thereafter. This is because the antenna's sensitivity rapidly decreases over 50° incident angles in accordance with the directive element pattern of the quasi-Yagi antenna. However, the DOA error retains reasonable accuracy within 5° up to $\pm 60°$ incident angle in a single-transmitter case in both ESPRIT and MUSIC. Thus, in a practical setup, three or four separate sets of antennas can cover the whole (360°) azimuth angle. The slight asymmetric error curve is predominantly due to the measurement environment. When multiple transmitter sources are used, the DOA error could be degraded from this value.

B. SDMA Performance in Two-Beam Simultaneous Beamforming

The purpose of this experiment is to demonstrate the SDMA capability or spatial channel selectivity of the proposed multibeam beamforming architecture. In this experiment, two-beam simultaneous beamforming has been tested using the eight-element array test-bed. The measurement is carried out in the open space of the laboratory room where strong reflections from the ceiling, floor, pillars, and walls surrounding the receiver are expected. Two unmodulated equal-power RF transmitters (Tx1 and Tx2) are set up in the same distance from the test-bed receiver. Before measurement, the circuit phase errors of the RF front-end are calibrated.

Fig. 12 shows the measured two-beam simultaneous beamforming results with respect to various combinations on locations of two RF sources. Angular difference between two RF transmitters is 20°, 30°, 50°, and 70°, respectively. The solid plots represent the measured antenna patterns from the weighted outputs, while the dotted plots exhibit the estimated array factors of the eight-element array antenna based on applied weighting coefficients.

The measured peak and null steering errors are within 3° accuracy with respect to the actual source locations. The measured peak-to-null interference suppressions are from 18 to 27 dB. The performance on peak/null steering and interference suppression is not obviously affected by the angular difference of two transmitters. The measured patterns exhibit good agreement with estimated array factors from a $-40°$ to $+40°$ angle, even when two transmitters are located in the smallest angular difference of 20°. As the angle increases over $\pm 40°$, the measured patterns still follow curves of the estimated patterns, but the positions of the higher order sidelobes and nulls gradually move away from the estimated angles. In higher incident angles, the SNR degradation due to the rapid decrease of the element antenna gain causes phase errors in the weighting process, leading to positioning errors. These positioning errors may be alleviated if a closed-loop circuit architecture is utilized to continuously optimize and update weighting coefficients for maximum signal-to-noise-plus-interference ratio (SNIR) by sampling beamformer outputs and feeding those back to the DSP controller.

Table I summarizes the DOA estimation errors using the ESPRIT algorithm, and interference suppressions from the measured antenna patterns with respect to the source locations. The measured DOA estimation errors with respect to the actual source directions are less than 2.5°. Overall, the multibeam-forming architecture retains reasonable accuracy in peak and null positioning and over 18-dB interference suppression for receiving two beams from 20° to 70° angular difference. This indicates that the digitally controlled DDS and analog beamformer ensure small errors in multitone weighting and its multiplication process and make this architecture practical as a low-cost high-speed multibeam adaptive antenna system.

C. Two-Channel Data Recovery by Spatial Filtering

A measurement of the two-channel simultaneous data recovery is carried out using the two RF transmitters positioned at $+40°$ (Tx1) and $-30°$ (Tx2). Two RF source signals are modulated by 25-Mb/s binary phase-shift keying (BPSK) with a common RF carrier at 5.8 GHz and are simultaneously transmitted at the same power. Different baseband data with the same data rate are used for Tx1 and Tx2 to demonstrate the two-channel simultaneous data recovery. The baseband data for Tx1 is a 23-bit pseudorandom binary sequence (PRBS) (PRBS: PN-23) code, and the code transmitted by Tx2 is a periodic binary code. In the test-bed receiver, the weighting coefficients are applied to the DDS to detect Tx1 baseband data at channel-1 output and Tx2 data at channel-2 output.

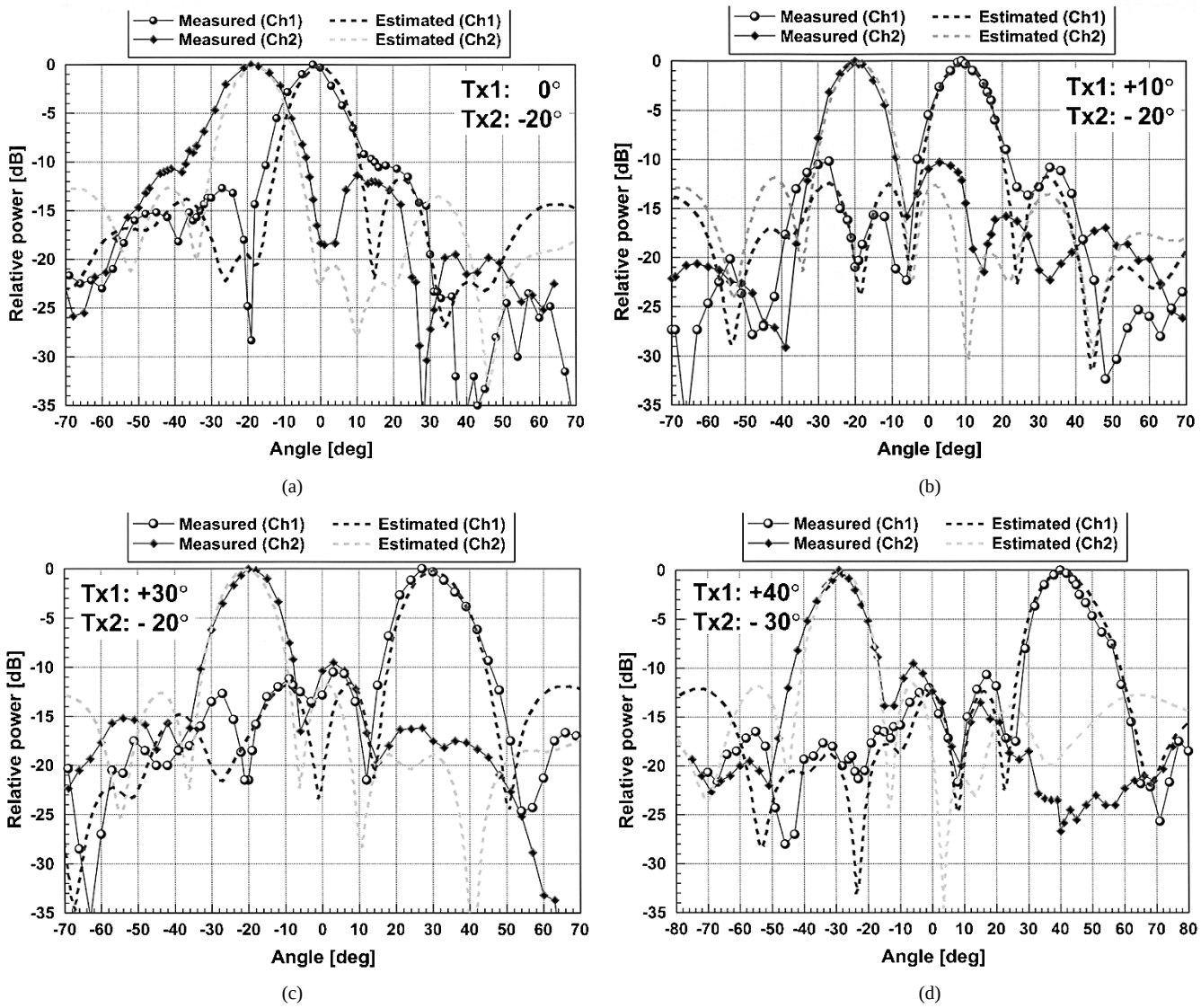

Fig. 12. Measured patterns of two-beam simultaneous beamforming. (a) Source locations: Tx1: 0°, Tx2: −20°, angular difference: 20°. (b) Source locations: Tx1: +10°, Tx2: −20°, angular difference: 30°. (c) Source locations: Tx1: +30°, Tx2: −20°, angular difference: 50°. (d) Source locations: Tx1: +40°, Tx2: −30°, angular difference: 70°.

TABLE I
DOA ESTIMATION ERRORS AND INTERFERENCE SUPPRESSIONS IN TWO-BEAM SIMULTANEOUS BEAMFORMING

Location of Tx 1 (Ch1 DOA est. error)	Location of Tx 2 (Ch2 DOA est. error)	Interference suppression in Ch 1 output	Interference suppression in Ch 2 output
0° (-1.2°)	-20° (+2.1°)	27 dB	18 dB
+10° (-0.6°)	-20° (+1.3°)	20.5 dB	21 dB
+30° (-2.1°)	-20° (+1.8°)	22 dB	18 dB
+40° (-1.6°)	-30 ° (+2.5°)	20 dB	27 dB

Fig. 13 shows the simultaneously recovered time-domain baseband data waveforms from the channel-1 (Ch1) and channel-2 (Ch2) outputs of the multibeam beamformer. The baseband data are properly extracted with slight signal distortions due to the bandwidth limitation of the 30-MHz LPFs placed on the output stage of the multibeam beamformer. Two-channel data recovery with 25 Mb/s is successfully demonstrated by the spatial filtering of the proposed multibeam adaptive antenna system given the condition where the desired signal and interference are transmitted at the same power.

D. BER Performance

The BER is tested to explore the impact of the interference signal under different SNR conditions on the desired signal, while multibeam beamforming is performed. The input or transmitted RF source is modulated in BPSK modulation. A non-return-to-zero (NRZ) 23-bit PRBS (PN-23) with 25-Mb/s data rate is generated by the BER tester and is used as a baseband data of the desired signal. Noise (noise bandwidth: 3 GHz) whose power is controlled by the RF amplifiers and variable attenuators is added to the modulated RF signal (signal bandwidth:

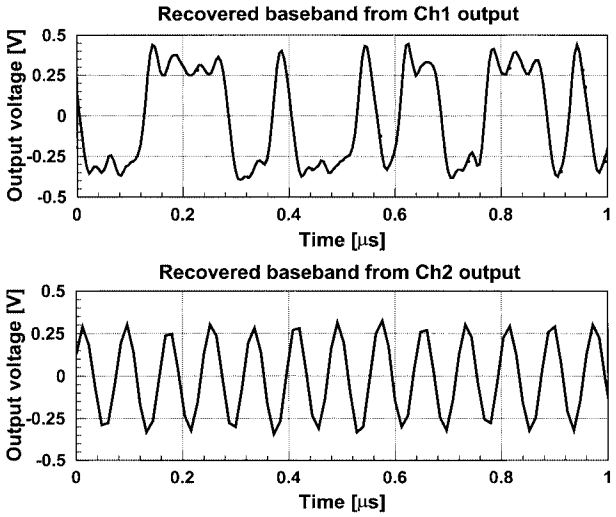

Fig. 13. Recovered baseband data in measurement of two-beam simultaneous beamforming. (Tx1 location: $+40°$, Tx2 location: $-30°$, both modulated in 5.8-GHz BPSK with 25-Mb/s data rate).

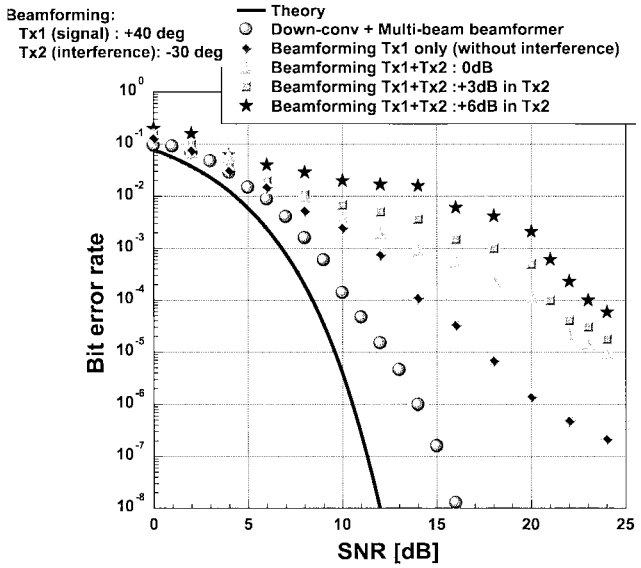

Fig. 14. Measured BER performance. The SNR condition of the desired signal and the interference power are simultaneously varied when two-beam simultaneous beamforming is performed.

70 MHz) for SNR control. The SNR is well defined from the power spectral density and bandwidth of signal and noise since the noise power spectral density is flat within the receiving IF bandwidth.

Fig. 14 shows the measured BER performance plotted with the theoretical estimation in BPSK modulation. First, the BER performance of the receiver (down-converter + multibeam beamformer) is measured from the in-phase RF input signals modulated by the 25-Mb/s 23-bit PRBS. The measured receiver BER exhibits good agreement with the theoretical curve, although around 2-dB degradation in SNR from the theoretical BPSK curve is observed. The noise figure of the RF LNAs mainly contributes this degradation.

Next, the BER performance under two-beam simultaneous beamforming is measured. As shown in Fig. 15, two independent RF sources are located at $+40°$ and $-30°$, respectively. The transmitter source 1 (Tx1) generates the modulated RF signal

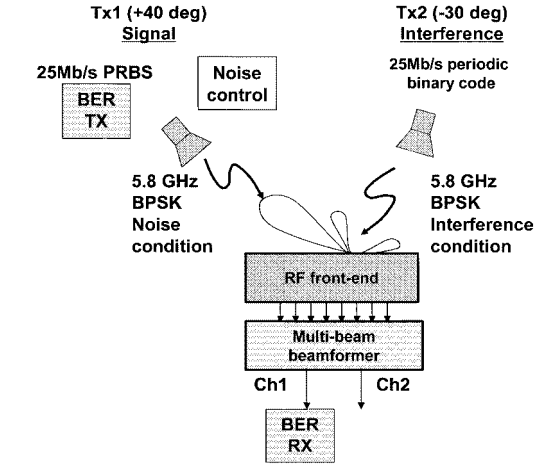

(a)

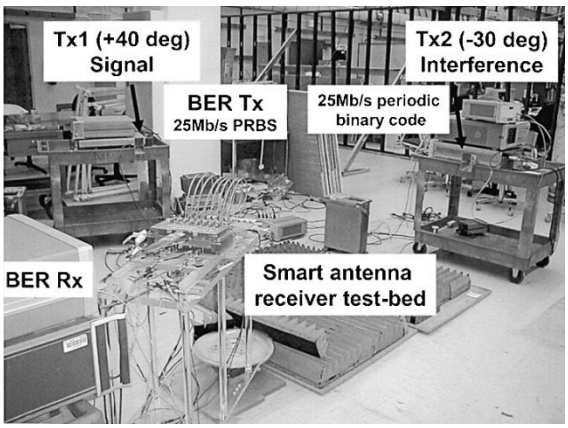

(b)

Fig. 15. BER measurement setup for beamforming. (a) Schematic diagram of the setup. (b) Photograph of the setup.

in BPSK by 25-Mb/s 23-bit PRBS from the BER tester, while the transmitter source 2 (Tx2) transmits the modulated one in BPSK by 25-Mb/s periodic binary code. Both RF signals contain a common RF carrier at 5.8 GHz. In this measurement, Tx1 is considered as a desired signal, whereas Tx2 is considered as an interference signal.

These two modulated RF signals are simultaneously transmitted and received at the multibeam smart antenna system performing two-beam simultaneous beamforming where the channel-1 output steers a peak toward a desired signal at $+40°$ and creates a null at $-30°$, while the channel-2 output performs peak and null steering in an opposite way. Under this condition, the BER performance of the demodulated PRBS baseband at the channel-1 output of the multibeam beamformer is observed, while the SNR condition of the desired RF signal in Tx1 is changed. The interference power in Tx2 is also varied to create a strong interference environment.

First, the BER in beamforming without an interference signal (no transmission in Tx2) is observed as a reference. Without interference, around 3-dB degradation in SNR is observed to obtain BER of 10^{-4}, as compared with the receiver only. This is due to the additional antenna noise and the SNR degradation during the RF signal transmission.

As the relative power of interference-to-signal (Tx2 to Tx1) increases from 0 to +6 dB, the BER degrades corresponding

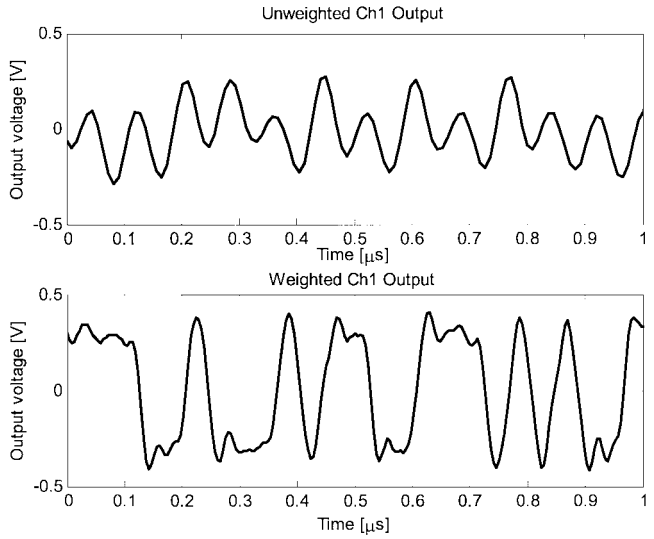

Fig. 16. Demodulated baseband data at channel-1 output with and without beamforming under strong interference ($\mathrm{SIR} = 0$ dB) and low noise ($\mathrm{SNR} = 25$ dB) conditions. The unweighted output is strongly influenced by the interference that includes the periodic binary code.

to the SNR impairment by increased interference power, but communication of the desired signal can be still established. The impact of strong interference is observed from the demodulated signals in Fig. 16. The upper frame shows the unweighted channel-1 output, whereas the lower one exhibits the weighted output, when the signal-to-interference ratio (SIR) is 0 dB with 25-dB SNR of the desired signal. Since obvious communication failure is observed without beamforming even at 0-dB SIR; this indicates an advantage of the spatial filtering in smart antenna systems by performing main-beam and null steering. As seen from Fig. 14, higher SNR of the desired signal is necessary to retain high communication quality (low BER) under strong interference. When the interference RF power is 6 dB over that of the desired signal, the BER curve degrades around 2 dB in SNR for BER of 10^{-4}, as compared with the case that the desired signal and interference are the same power. The system achieves BER of 10^{-4} at 14-dB SNR with no interference, and at 20-dB SNR with 0-dB SIR, respectively, without any error correction coding.

VI. Conclusion

A new system architecture of the multibeam adaptive array has been presented. The proposed analog–digital hybrid beamforming approach is capable of high-speed real-time multibeam construction in multichannel wireless communication applications. A test-bed based on two beams, and having eight antenna elements has been developed. The 5.8-GHz test-bed successfully demonstrates the two-beam simultaneous beamforming. The DOA estimation and peak/null steering achieve within 2.5° and 3° accuracy from the actual source locations, yet the interference suppression holds 18–27 dB, when the RF signals from two transmitters located 20° to 70° angular difference are simultaneously received. Data throughput of 25 Mb/s in each channel has been demonstrated in a two-channel baseband data recovery test for SDMA capability. The BER measurement under two-beam beamforming exhibits robustness of the system under strong interference and a noisy environment by using spatial filtering. It is expected that the proposed architecture can be developed to satisfy the need of high data rate and robust communication for SDMA applications.

Acknowledgment

The authors would like to thank Dr. S.-S. Jeon, currently with the Microsemi Corporation, Los Angeles, CA, for his help with our measurements.

References

[1] J. Razavilar, F. Rashid-Farrokhi, and K. J. R. Liu, "Software radio architecture with smart antennas: A tutorial on algorithms and complexity," *IEEE J. Select. Areas Commun.*, vol. 17, pp. 662–676, Apr. 1999.

[2] K. Sheikh, D. Gesbert, D. Gore, and A. Paulraj, "Smart antennas for broadband wireless networks," *IEEE Commun. Mag.*, pp. 100–105, Nov. 1999.

[3] G. Tsoulos, M. Beach, and J. McGeehan, "Wireless personal communications for the 21st Century: European technological advances in adaptive antennas," *IEEE Commun. Mag.*, pp. 102–107, Sept. 1997.

[4] C. B. Dietrich, W. L. Stutzman, B.-K. Kim, and K. Dietze, "Smart antennas in wireless communications: Base-station diversity and handset beamforming," *IEEE Antennas Propagat. Mag.*, vol. 42, pp. 142–151, Oct. 2000.

[5] R. T. Compton, *Adaptive Antennas: Concepts and Performance*. Englewood Cliffs, NJ: Prentice-Hall, 1988.

[6] C. Godara, "Application of antenna arrays to mobile communications, part II: Beam-forming and direction-of-arrival considerations," *Proc. IEEE*, vol. 85, pp. 1195–1245, Aug. 1997.

[7] J. Wu, "Smart antenna system implementation based on digital beam-forming and software radio technologies," in *IEEE MTT-S Int. Microwave Symp. Dig.*, vol. 1, June 2002, pp. 323–326.

[8] S. S. Jeon, Y. Wang, Y. Qian, and T. Itoh, "A novel smart antenna system implementation for broad-band wireless communications," *IEEE Trans. Antennas Propagat.*, vol. AP-50, pp. 600–606, May 2002.

[9] S. S. Jeon, J. Y. Park, Y. Wang, and T. Itoh, "A broadband beamformer for millimeter-wave systems using sub-band sampling," in *IEEE MTT-S Int. Microwave Symp. Dig.*, vol. 1, June 2003, pp. 579–582.

[10] Y. Qian, W. R. Deal, N. Kaneda, and T. Itoh, "A uniplanar quasi-Yagi antenna with wide bandwidth and low mutual coupling characteristics," in *IEEE AP-S Int. Symp. Dig.*, July 1999, pp. 924–927.

[11] R. H. Roy and T. Kailath, "ESPRIT—Estimation of signal parameters via rotational invariance techniques," *IEEE Trans. Acoust., Speech, Signal Processing*, vol. ASSP-37, pp. 984–995, July 1989.

[12] I. S. Reed, J. D. Mallett, and L. E. Brennan, "Rapid convergence rate in adaptive arrays," *IEEE Trans. Aerosp. Electron. Syst.*, vol. AES-10, pp. 853–863, Nov. 1974.

[13] R. O. Schmidt, "Multiple emitter location and signal parameter estimation," *IEEE Trans. Antennas Propagat.*, vol. AP-34, pp. 276–280, Mar. 1986.

Takahide Nishio (S'00) was born in Hamamatsu, Japan, in 1972. He received the B.S. degree in electronic and communication engineering from Meiji University, Tokyo, Japan, in 1994, the M.S. degree in electronic engineering from Shizuoka University, Hamamatsu, Japan, in 1996, and the Ph.D. degree in electrical engineering from University of California at Los Angeles (UCLA), in 2003.

In 1996, he joined the Japan Defense Agency, Tokyo, Japan, where he has been a Technical Official with the Technical Research and Development Institute. From 2002 to 2003, he was a Graduate Student Researcher (Research Assistant) with the Department of Electrical Engineering, UCLA. His research interests include phased-array antennas, adaptive beamforming arrays, and smart antenna systems for microwave and millimeter-wave radars and wireless communications.

Dr. Nishio was a recipient of the Honorable Mention Award in the Student Paper Competition of the 2003 IEEE Microwave Theory and Techniques Society (IEEE MTT-S) International Microwave Symposium.

Hsiao-Ping Tsai (S'00–M'03) received the M.S. degrees in electrical engineering from the National Taiwan University, Taiwan, R.O.C., in 1997, and the Ph.D. degree in electrical engineering from University California at Los Angeles (UCLA), in 2002.

From 1997 to 1998, she was a Teaching Assistant with the National Taiwan University. From May to July 2002, she was a Post-Doctoral Researcher with UCLA, where she conducted research on simulation of semiconductor devices for integrated-circuit (IC) design. Since August 2002, she has been a Package Application Engineer with Mindspeed Technologies, Newport Beach, CA. Her research interests include the time-domain full-wave modeling of nonlinear semiconductor devices and microwave circuits.

Dr. Tsai was the recipient of the Honorable Mention Award of the Student Paper Competitions of the IEEE Microwave Theory and Techniques Society (IEEE MTT-S) International Microwave Symposium in 2000 and 2002.

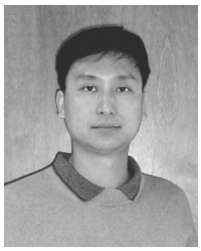

Yuanxun Wang (S'96–M'99) received the B.S. degree in electrical engineering from the University of Science and Technology of China (USTC), Hefei, China, in 1993, and the M.S. and Ph.D. degrees in electrical engineering from the University of Texas at Austin, in 1996 and 1999, respectively.

From 1995 to 1999, he was a Research Assistant with the Department of Electrical and Computer Engineering, University of Texas at Austin. From 1999 to 2002, he was a Research Engineer and Lecturer with the Department of Electrical Engineering, University of California at Los Angeles (UCLA), prior to joining the faculty. Since 2002, he has been an Assistant Professor with the Electrical Engineering Department, UCLA. He has authored and coauthored over 60 refereed journal and conference papers. His research has focused on high-performance antenna array and microwave amplifier systems for wireless communication and radar, as well as numerical modeling techniques. His current research interests feature the fusion of signal processing and circuit techniques in microwave system design.

Dr. Wang is a member of the International Society for Optical Engineers (SPIE).

Tatsuo Itoh (S'69–M'69–SM'74–F'82) received the Ph.D. degree in electrical engineering from the University of Illinois at Urbana-Champaign, in 1969.

From September 1966 to April 1976, he was with the Electrical Engineering Department, University of Illinois at Urbana-Champaign. From April 1976 to August 1977, he was a Senior Research Engineer with the Radio Physics Laboratory, SRI International, Menlo Park, CA. From August 1977 to June 1978, he was an Associate Professor with the University of Kentucky, Lexington. In July 1978, he joined the faculty at The University of Texas at Austin, where he became a Professor of Electrical Engineering in 1981 and Director of the Electrical Engineering Research Laboratory in 1984. During the summer of 1979, he was a Guest Researcher with AEG-Telefunken, Ulm, Germany. In September 1983, he was selected to hold the Hayden Head Centennial Professorship of Engineering at The University of Texas at Austin. In September 1984, he was appointed Associate Chairman for Research and Planning of the Electrical and Computer Engineering Department, The University of Texas at Austin. In January 1991, he joined the University of California at Los Angeles (UCLA) as Professor of Electrical Engineering and Holder of the TRW Endowed Chair in Microwave and Millimeter Wave Electronics. He was an Honorary Visiting Professor with the Nanjing Institute of Technology, Nanjing, China, and at the Japan Defense Academy. In April 1994, he was appointed an Adjunct Research Officer with the Communications Research Laboratory, Ministry of Post and Telecommunication, Japan. He currently holds a Visiting Professorship with The University of Leeds, Leeds, U.K. He has authored or coauthored 310 journal publications, 640 refereed conference presentations, and has written 30 books/book chapters in the area of microwaves, millimeter waves, antennas, and numerical electromagnetics. He has generated 60 Ph.D. students.

Dr. Itoh is a member of the Institute of Electronics and Communication Engineers of Japan, and Commissions B and D of USNC/URSI. He served as the editor of the IEEE TRANSACTIONS ON MICROWAVE THEORY AND TECHNIQUES (1983–1985). He serves on the Administrative Committee of the IEEE Microwave Theory and Techniques Society (IEEE MTT-S). He was vice president of the IEEE MTT-S in 1989 and president in 1990. He was the editor-in-chief of IEEE MICROWAVE AND GUIDED WAVE LETTERS (1991–1994). He was elected an Honorary Life Member of the IEEE MTT-S in 1994. He was elected a member of the National Academy of Engineering in 2003. He was the chairman of the USNC/URSI Commission D (1988–1990) and chairman of Commission D of the International URSI (1993–1996). He is chair of the Long Range Planning Committee of the URSI. He serves on advisory boards and committees of a number of organizations. He has been the recipient of numerous awards including the 1998 Shida Award presented by the Japanese Ministry of Post and Telecommunications, the 1998 Japan Microwave Prize, the 2000 IEEE Third Millennium Medal, and the 2000 IEEE MTT-S Distinguished Educator Award.